

Channel Capacity of Magnetic Induction Based Wireless Underground Sensor Networks under Practical Constraints

S. Kisseleff, W. Gerstacker, R. Schober
 Institute for Digital Communications
 Friedrich-Alexander University
 Erlangen-Nuremberg, Germany
 Email: {kisseleff, gersta, schober}@lnt.de

Z. Sun
 Department of Electrical Engineering
 State University of New York at Buffalo
 Buffalo, NY, USA
 Email: zhisun@buffalo.edu

I. F. Akyildiz
 Broadband Wireless Networking Lab
 Georgia Institute of Technology
 Atlanta, USA
 Email: ian.akyildiz@ee.gatech.edu

Abstract—Wireless Underground Sensor Networks (WUSNs) present a variety of new research challenges. Recently a magneto-inductive (MI) waveguide technique has been proposed to overcome the very harsh propagation conditions in WUSNs. In this approach, several resonant relay circuits are deployed between the two nodes to be connected. This technique allows for an extension of the transmission range, which can be quite limited, if relays are not deployed. In this paper, channel and noise models for MI-WUSNs using MI-waveguides are developed. Results of a numerical evaluation of the channel capacity under practical constraints are provided and the influence of the system parameters on the performance is discussed.

I. INTRODUCTION

Wireless underground sensor networks (WUSNs) are an emerging and promising research area. Here, the goal is to establish efficient wireless communication in the underground medium. Typical applications for such networks include soil condition monitoring, earthquake prediction, border patrol, etc. [1], [2]. Since the propagation medium is soil, rock, and sand, traditional wireless signal propagation techniques using electromagnetic (EM) waves can be only applied for very small transmission ranges due to high pathloss and vulnerability to changes of soil properties, such as soil moisture [3], [4]. Magnetic induction (MI)-based WUSNs were first introduced in [2]. MI-WUSNs make use of magnetic antennas implemented as coils, which are combined in waveguide structures with several passive relay devices between two transceiver nodes [5]. Similar to traditional wireless relaying concepts this approach is supposed to benefit from a lower pathloss. Hence, the transmission range can be greatly improved compared to the EM based approach. A distinct advantage of MI relays is that these devices do not need any power supply, so that the energy has to be provided only in the transceiver nodes. The transceiver nodes can be recharged by removable or mobile aboveground devices [6]. Although WUSN applications generally do not require high data rates [2], it is essential to analyze the channel capacities of MI-WUSNs in order to be able to provide sufficient performance. For this analysis, a reliable and comprehensive system model is indispensable. In previous work, some efforts were made to characterize the channel conditions of MI-based transmission. Magneto-inductive waveguides for metamaterials were considered in [7] and [8], where the signal is described as an MI wave traveling

through the channel. Based on this, in [9], a corresponding noise model was proposed. However, these works are not directly related to WUSNs, but to metamaterials and several assumptions were made, which do not hold for WUSNs, e.g. very small coil sizes, small distances between relays (only a few centimeters), and no influence of the environment on the quality of transmission. In [5], an MI-WUSN channel model with frequency-selective pathloss was proposed. In [10], analytical expressions for the bandwidth and channel capacity of MI waveguides and waveguide networks were presented. However, these expressions are based on the simplifications, which hold only for narrowband transmissions and limited magnetic induction. In [5] and [10], the following assumptions were made: 1) The pathloss does not depend on the soil properties, i.e., additional losses due to the medium were not taken into account. 2) An additive white Gaussian noise channel was assumed. 3) The carrier frequency and other system parameters were not optimized. 4) There were no restrictions on the circuit elements of the relay devices and transceiver circuits. Although these assumptions allow for a simple system design, they are not valid for practical systems. Therefore, in order to provide a more realistic system model, we have to fully or partially drop these assumptions. In this paper, we address the following issues: 1) We take into account the influence of conductivity-based losses in the soil, which are not negligible at high frequencies. 2) We analyze the frequency-selective pathloss and the received noise power for MI-waveguides. 3) We consider the channel capacity of the waveguides for optimum selection of the available system parameters. To this end, we formulate and solve an optimization problem. 4) The choice of the circuit elements at the relays, the deployment strategies, and their influence on the optimization results is discussed. The theoretical considerations provided here are essential for a basic understanding of MI-waveguides and for the reliable design of practical MI-WUSNs.

This paper is organized as follows. In Section II, a novel system model for MI-WUSNs is presented. Section III gives insight into the optimization of the system parameters for maximization of the channel capacity between two underground sensor nodes. Numerical results are discussed in Section IV. Finally, Section V concludes the paper.

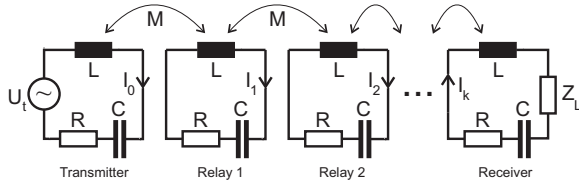


Fig. 1. Block diagram of MI-waveguide with transmitter, receiver, and $(k-1)$ relays.

II. SYSTEM MODELING

In this section, a step-by-step development of the system model is presented. Similar to [5], we assume that the waveguide structure contains one transmitter circuit with a voltage source U_t , one receiver circuit with a load impedance Z_L , and $(k-1)$ passive relays, which are placed equidistantly between the transceivers. Each circuit includes a magnetic antenna (which in this work is assumed to be a multilayer air core coil), a capacitor C , and a resistor R (which models the copper resistance of the coil), see Fig. 1. In this work, we do not consider parasitic effects (skin effect in windings, proximity effect, parasitic capacities), which may occur in circuit elements at very high frequencies. We assume that in the considered frequency ranges the influence of these effects is negligible. Because all involved signal mappings are linear for magnetic induction based transmissions, a linear channel model results. The inductivity of a multilayer coil is given by [11], [12]

$$L = \frac{21\mu N^2 a}{4\pi} \left(\frac{a}{l+h} \right)^{0.5}, \quad (1)$$

where N denotes the number of windings, a is the radius of the coil, $l = 0.5a$ is the length of the coil [11], h is the height of the windings over the coil surface, and μ denotes the permeability of the soil. The capacitance of the capacitor is chosen to make each circuit resonant at frequency f_0 [5], i.e., $C = \frac{1}{(2\pi f_0)^2 L}$. The copper resistance of the coil is given by [11]

$$R = \rho \cdot \frac{l_w}{A_w} = \rho \cdot \frac{2aN}{r_w^2}, \quad (2)$$

where $\rho \approx 1.678 \cdot 10^{-2} \Omega \cdot \text{mm}^2/\text{m}$ is the copper resistivity, l_w denotes the total wire length, A_w is the cross-section area of the wire, and r_w is the radius of the wire. The induced voltage is related to the coupling between the coils, which is determined by the mutual inductance [10]

$$M = \mu\pi N^2 \frac{a^4}{4r^3} (2 \sin \theta_t \sin \theta_r + \cos \theta_t \cos \theta_r) \cdot G, \quad (3)$$

where r denotes the distance between two coils, and θ_t and θ_r are the angles between the coil radial directions and the line connecting the two coil centers, respectively. G is an additional loss factor due to eddy currents. We assume that all devices are deployed in a homogeneous conductive environment (soil) with constant properties over space and time.

A. Losses in the Soil

From the basics of electromagnetism, eddy currents cause additional attenuation of the magnetic field [13]. Eddy currents result from changes in the magnetic field, similar to the skin effect in wires. Such losses have been neglected in [5], [10] due

to their small impact for very low carrier frequencies. However, in this work, we need to consider this effect as well, since the carrier frequency is one of the optimization parameters, see Section III-A. Therefore, we introduced a scaling factor $G = e^{-r/\delta}$ in (3), which represents the attenuation of the magnetic field [14] and therefore the attenuation of the magnetic flux and mutual inductance. This attenuation factor depends on the skin depth δ for conductive materials [14]

$$\delta = \frac{1}{2\pi f \sqrt{\frac{\mu\epsilon}{2} \left(\sqrt{1 + \frac{\sigma^2}{(2\pi f)^2 \epsilon^2}} - 1 \right)}}, \quad (4)$$

where ϵ and σ denote the permittivity and conductivity of the soil, respectively, and f is the signal frequency. Note that we do not utilize the simplified version of the skin depth, given by the well-known formula $\delta \approx \sqrt{\frac{1}{\pi f \mu \sigma}}$, which holds only for good conductors, because in our case, we consider a wide range of frequencies, for which the soil may be a poor conductor.

B. Pathloss

We assume that all coil axes are turned in the same direction. Due to skin effect, the magnetic flux is greatly attenuated in the conductive material of the coil and allows only transmissions between the neighbor coils. The voltage in coil n induced by coil $n-1$ is $U_n = j2\pi f M \cdot I_{n-1}$, where j stands for the imaginary unit. This leads to the following voltage equation in the relay circuits, see Fig. 1:

$$\left(j2\pi f L + \frac{1}{j2\pi f C} + R \right) \cdot I_n - j2\pi f M \cdot (I_{n-1} + I_{n+1}) = 0. \quad (5)$$

After reordering, we obtain from (5)

$$I_{n+1} = \frac{Z}{j2\pi f M} \cdot I_n - I_{n-1} = x \cdot I_n - I_{n-1}, \quad (6)$$

where $Z = j2\pi f L + \frac{1}{j2\pi f C} + R$ and $x = \frac{Z}{j2\pi f M}$. Since the receiver circuit is only influenced by one relay, its voltage equation is slightly different and given by

$$\left(j2\pi f L + \frac{1}{j2\pi f C} + R \right) \cdot I_k + Z_L \cdot I_k - j2\pi f M \cdot I_{k-1} = 0, \quad (7)$$

which leads to

$$I_k = \frac{1}{x + x_L} \cdot I_{k-1}, \quad (8)$$

with $x_L = \frac{Z_L}{j2\pi f M}$. Using (6) and (8) we can express I_k as a function of I_m similar to [10]

$$I_k = \frac{1}{S(x, x_L, k-m)} \cdot I_m, \quad \forall m, \quad (9)$$

$$S(x, x_L, n) = F(x, n) + x_L \cdot F(x, n-1), \quad (10)$$

$$F(x, n) = x \cdot F(x, n-1) - F(x, n-2), \quad n \geq 2, \quad (11)$$

$$F(x, 1) = x, \quad F(x, 0) = 1. \quad (12)$$

From the difference equation (11), (12), a closed-form solution for $F(x, n)$ can be obtained as

$$F(x, n) = \frac{\left(\frac{x + \sqrt{x^2 - 4}}{2} \right)^{n+1} - \left(\frac{x - \sqrt{x^2 - 4}}{2} \right)^{n+1}}{\sqrt{x^2 - 4}}. \quad (13)$$

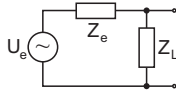


Fig. 2. Equivalent circuit for modeling MI-waveguide receiver-side.

For the transmitter circuit, we can express the transmitter current I_0 as a function of the voltage source U_t as

$$U_t = Z \cdot I_0 - j2\pi f M \cdot I_1, \quad (14)$$

From (9), we have

$$I_1 = \frac{S(x, x_L, k-1)}{S(x, x_L, k)} \cdot I_0, \quad (15)$$

which can be employed in (14) to obtain

$$\frac{U_t}{j2\pi f M} = I_0 \left(\frac{x \cdot S(x, x_L, k) - S(x, x_L, k-1)}{S(x, x_L, k)} \right). \quad (16)$$

Using (9) and (16) we get

$$I_k = \frac{U_t}{j2\pi f M} \cdot \frac{1}{S(x, x_L, k+1)}. \quad (17)$$

Thus, the active received power¹ at Z_L can be expressed as

$$P_r(f) = \frac{1}{2} |I_k|^2 \operatorname{Re}\{Z_L\} = \frac{|U_t|^2 \cdot \operatorname{Re}\{Z_L\}}{2 |j2\pi f M|^2 |S(x, x_L, k+1)|^2}. \quad (18)$$

Exploiting (16), the required transmit power² is

$$P_t(f) = \frac{1}{2} |U_t \cdot I_0| = \frac{1}{2} \frac{|U_t|^2}{|j2\pi f M|} \frac{|S(x, x_L, k)|}{|S(x, x_L, k+1)|}. \quad (19)$$

Thus, from (18) and (19) the resulting pathloss is

$$L_p(f) = \left| \frac{P_t(f)}{P_r(f)} \right| = \frac{|S(x, x_L, k) \cdot S(x, x_L, k+1)|}{|\operatorname{Im}\{x_L\}|}. \quad (20)$$

For $|Z| \gg |j2\pi f M|$ the pathloss function in (20) is similar to that proposed in [5] and [10]. $|Z| \gg |j2\pi f M|$ implies a low mutual induction or a low carrier frequency, which yields low channel capacity for such MI-waveguides, see Section IV. For a larger mutual induction and higher carrier frequencies, the pathloss in (20) differs significantly from that in [5] and [10], due to the simplified assumptions for the transmit power calculations [5] and due to the influence of the load impedance, which was neglected in [10].

C. Load Impedance

The active received power in (18) can be rewritten as

$$P_r(f) = \frac{1}{2} \frac{|U_t|^2}{|F(x, k)|^2} \cdot \frac{\operatorname{Re}\{Z_L\}}{\left| j2\pi f M \cdot \frac{F(x, k+1)}{F(x, k)} + Z_L \right|^2}. \quad (21)$$

If the received signal is modeled via the equivalent circuit shown in Fig. 2, the received power at Z_L is given by

¹Only the active part of the complex received power can be used for signal processing. $\operatorname{Re}\{\cdot\}$ and $\operatorname{Im}\{\cdot\}$ denote the real and imaginary part of a complex number, respectively.

²The total consumed power comprises both the active and the reactive parts.

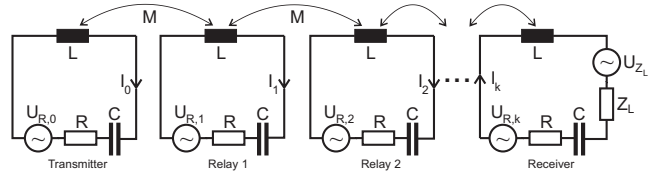


Fig. 3. Noise sources in the MI-waveguide.

$$P_r(f) = \frac{1}{2} |U_e|^2 \cdot \frac{\operatorname{Re}\{Z_L\}}{|Z_e + Z_L|^2}. \quad (22)$$

The powers in (21) and (22) are identical, if we choose $U_e = \frac{U_t}{F(x, k)}$ and $Z_e = j2\pi f M \cdot \frac{F(x, k+1)}{F(x, k)}$ for the equivalent voltage and the equivalent impedance, respectively. In order to minimize the power losses, the load impedance should be chosen such that reflections do not occur [15], i.e., $Z_{L, \text{opt}} = Z_e$. However, with increasing number of relays, the order of function $F(x, k)$ increases. The order of $Z_{L, \text{opt}}$ depends on this function and increases as well. Hence, the implementation of $Z_{L, \text{opt}}$ requires a complex passive circuit with a large number of elements. Since the elements of this circuit will be noisy, the received noise power may become very large and degrade the performance of the practical system. Therefore, it is advantageous to keep the load impedance as simple as possible. In the simplest case, the load impedance is matched only to the equivalent impedance Z_e at the carrier frequency using a resistor, i.e.,

$$Z_L = Z_{L, R} = \operatorname{Re} \left\{ j2\pi f_0 M \cdot \frac{F(x_0, k+1)}{F(x_0, k)} \right\}, \quad (23)$$

where $x_0 = \frac{R}{j2\pi f_0 M}$. Due to a very small bandwidth of MI-based systems [5], we have $|Z_{L, R} - Z_{L, \text{opt}}| \approx 0$, such that the loss in channel capacity using (23) is negligibly small.

D. Noise Modeling

For performance evaluation of MI-waveguides, the received noise power at the load impedance $Z_{L, R}$ is required. We assume thermal noise to be the dominant noise source, similar to [9]. There may be other sources of noise, which stem from the uncertainty of the environment, see the measurements in [4]. These noise processes are basically EM-waves, which may influence the magnetic field of the coils. However, due to the high attenuation of EM-waves in soil [3], [4], reflections, and an assumed sufficient depth of burial of e.g. at least 10 cm, the influence of ambient EM-waves is low. Therefore, in our considerations, we focus on the thermal noise, which is caused by the resistors in the relay and transceiver circuits. In each relay n , the influence of the noise from resistor R is modeled as an additional voltage source $U_{R, n}$, $n \in \{1, \dots, k-1\}$ [9]. We also assume a noise source in the transmitter and in the receiver, modeled as voltage sources $U_{R, 0}$ and $U_{R, k}$, respectively. In addition, we take into account the noise caused by load resistor $Z_{L, R}$ and model it as voltage source U_{Z_L} , see Fig. 3. Due to the superposition principle, we can first calculate the received noise power caused by the copper resistance of the coils including the transmitter and receiver coils, and then add the received noise power produced by the load resistor. The basic circuit equations become now

$$Z \cdot I_n - j2\pi f M \cdot (I_{n-1} + I_{n+1}) + U_{R,n} = 0, \quad (24)$$

$$I_{n+1} = x \cdot I_n - I_{n-1} + \frac{U_{R,n}}{j2\pi f M}, \quad (25)$$

$$I_k = \frac{1}{x + x_L} \cdot I_{k-1} - \frac{1}{x + x_L} \cdot \frac{U_{R,k}}{j2\pi f M}. \quad (26)$$

Following a similar procedure as in (9)-(17) we obtain

$$I_1 = I_0 \frac{S(x, x_L, k-1)}{S(x, x_L, k)} - \sum_{n=0}^{k-1} \frac{U_{R,k-n}}{j2\pi f M} \cdot \frac{S(x, x_L, n)}{S(x, x_L, k)} \quad (27)$$

$$I_0 = - \sum_{n=0}^k \left(\frac{U_{R,k-n}}{j2\pi f M} \cdot \frac{S(x, x_L, n)}{S(x, x_L, k+1)} \right). \quad (28)$$

After several substitutions and reordering steps, we get

$$I_k = - \sum_{m=0}^k \left(\sum_{n=0}^m \frac{U_{R,k-n}}{j2\pi f M} \frac{S(x, x_L, n)}{S(x, x_L, m)S(x, x_L, m+1)} \right). \quad (29)$$

Therefore, the noise power at the load resistor $Z_{L,R}$ is

$$P_{N,R}(f) = \frac{1}{2} \frac{Z_{L,R}}{|j2\pi f M|^2} \times \left| \sum_{m=0}^k \left(\sum_{n=0}^m U_{R,k-n} \frac{S(x, x_L, n)}{S(x, x_L, m)S(x, x_L, m+1)} \right) \right|^2. \quad (30)$$

If we assume statistically independent noise sources with the well-known Johnson-noise [16] power spectral densities $E\{|U_{R,n}(f)|^2\} = 4KTR$, $\forall n$, where $K \approx 1.38 \cdot 10^{-23}$ J/K is the Boltzmann constant, $T = 290$ K is the temperature in Kelvin, R is the copper resistance in (2), and $E\{\cdot\}$ denotes the expectation value, the average noise power caused by the copper resistors becomes

$$E\{P_{N,R}(f)\} = \frac{1}{2} \frac{4KTRZ_{L,R}}{|j2\pi f M|^2} \times \sum_{n=0}^k \left(|S(x, x_L, n)|^2 \left| \sum_{m=n}^k \frac{1}{S(x, x_L, m)S(x, x_L, m+1)} \right|^2 \right). \quad (31)$$

The influence of the noise caused by the load resistor, which has power spectral density $E\{|U_{Z_{L,R}}(f)|^2\} = 4KTZ_{L,R}$, can be calculated similarly as

$$E\{P_{N,Z_{L,R}}(f)\} = \frac{1}{2} \frac{4KTZ_{L,R}^2}{|j2\pi f M|^2} \times \left| \sum_{m=0}^k \frac{1}{S(x, x_L, m)S(x, x_L, m+1)} \right|^2. \quad (32)$$

Hence, the total noise power spectral density at the load resistor is given by

$$E\{P_{\text{noise}}(f)\} = E\{P_{N,R}(f)\} + E\{P_{N,Z_{L,R}}(f)\}. \quad (33)$$

III. CHANNEL CAPACITY

The channel capacity of MI-WUSNs depends on the waveguide parameters. Therefore, one of the major tasks in our investigations is to find optimal system parameters, which maximize the channel capacity.

A. Problem Formulation

In this paper, we choose three parameters, which can be easily adjusted, for the capacity maximization for a given number of relay devices: The transmit power density spectrum, the number of coil windings, and the carrier frequency. Other parameters, such as the capacitance of the relay capacitor or the soil properties either depend on the chosen parameters, or cannot be changed for a given environment. Our optimization problem can be formulated as follows:

$$\begin{aligned} \arg \max_{\forall f_0, N, P_t(f)} C_{ch} &= \int_{-\infty}^{+\infty} \log_2 \left(1 + \frac{P_t(f)}{L_p(f) E\{P_{\text{noise}}(f)\}} \right) df \\ \text{s.t.:} \quad (1) \quad &\int_{-\infty}^{+\infty} P_t(f) df = P, \quad (2) \quad N \in [N_{\min}, N_{\max}], \\ (3) \quad &f_0 \in [f_{0,\min}, f_{0,\max}], \quad (4) \quad \frac{1}{(2\pi f_0)^2 L} \geq C_0, \end{aligned} \quad (34)$$

where C_{ch} is the channel capacity [17] and P is the total transmit power. $P_t(f)$ denotes the transmit power spectral density, which can be adjusted via U_t . $L_p(f)$ and $E\{P_{\text{noise}}(f)\}$ are given by (20) and (33), respectively. The size of the relay devices can become a crucial factor for the deployment. Therefore, we restrict the number of windings to the interval $[N_{\min}, N_{\max}]$ (Constraint 2). Due to additional parasitic effects in coils (especially the skin effect and proximity effect [18]), which may occur at high frequencies, we also constrain the frequency range between $f_{0,\min} = 1$ kHz and $f_{0,\max} = 300$ MHz (Constraint 3). Moreover, a high carrier frequency combined with a high number of windings implies a very low capacitance. Unfortunately, for low capacitances the parasitic resistance in the capacitor [19] becomes substantial and leads to a mismatch at the resonance frequency, which may dramatically change the properties of the system. Therefore, we impose a lower bound C_0 on the capacitance (Constraint 4, ‘‘capacitor constraint’’).

B. Proposed Optimization Algorithm

An explicit approximate solution for problem (34) can be given only for the case, when the magnetic induction in the coils is very low. This assumption allows to simplify and solve the problem analytically. Unfortunately, this case is not practically relevant because of the associated low channel capacity. Therefore, we have to find the optimal solution by numerical evaluation. The optimization problem is not convex, as is obvious from Fig. 4a). Hence, the standard convex optimization tools [20] are not applicable.

Here, we propose the following algorithm for solving (34). In the two-dimensional space (region of interest), a grid is spanned between the minimum and maximum values of f_0 and N . For each point of the grid, the corresponding channel capacity is determined. In order to enhance the precision of the optimization result, X_I iterations of the algorithm are applied. In each iteration a region of interest is determined based on the point with the largest channel capacity. In the first iteration, the limits of f_0 and N are given by the constraints in (34). We set the number of points in the f_0 -direction to 40 and in the N -direction to 10. Due to a large difference between the maximum and the minimum value of f_0 , the distances between the points of the grid in the f_0 -direction are not selected as equal, but

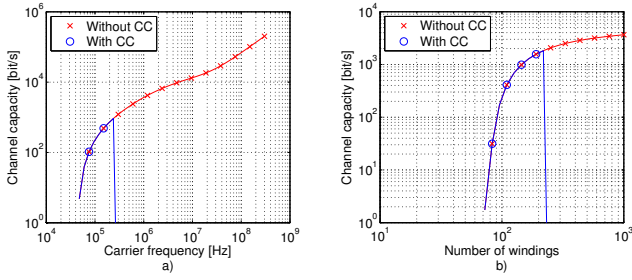


Fig. 4. a) Channel capacity vs. carrier frequency for constant number of windings; b) Channel capacity vs. number of windings for constant carrier frequency.

exponentially increasing. If the point does not satisfy Constraint 4, the channel capacity is set to zero. In order to calculate the channel capacity for each of the remaining points, we first determine the optimal transmit power spectral density $P_t(f)$, for which the channel capacity is maximized, using water filling [17], i.e.,

$$P_t(f) = \max \left(\left(\frac{1}{\lambda} - L_p(f) E\{P_{\text{noise}}(f)\} \right), 0 \right), \quad (35)$$

where λ is adjusted to meet Constraint 1. The integration in (34) is carried out numerically using Simpson's rule, which yields the channel capacity for a given (f_0, N) -point of the grid.

IV. NUMERICAL RESULTS

In this section, we discuss the results for the simulated channel capacity of different waveguide constellations. In our simulations, we assume a total transmit power of $P = 10$ mW. Furthermore, we utilize coils with wire radius $r_w = 0.5$ mm and coil radius $a = 0.15$ m. The conductivity is $\sigma = 0.01$ S/m for dry soil and $\sigma = 0.077$ S/m for wet soil in this work. The permittivity value is $\epsilon = 7\epsilon_0$ and $\epsilon = 29\epsilon_0$ for dry and wet soil, respectively, where $\epsilon_0 \approx 8.854 \cdot 10^{-12}$ F/m is the electric constant. Since the permeability of soil is close to that of air, we use $\mu = \mu_0$ with the magnetic constant $\mu_0 = 4\pi \cdot 10^{-7}$ H/m. We analyzed two different deployment schemes: Horizontal axes deployment (when the coil axes are identical to the waveguide axis) and vertical axes deployment (when the coil axes are turned to the ground surface) as proposed in [10]. For vertical axes deployment, $\theta_t = \theta_r = 0$ and for horizontal axes deployment, $\theta_t = \pi/2$ and $\theta_r = -\pi/2$ are used, to maintain the correct direction of the current flow in the relay circuits. The advantage of the vertical axes deployment is the omnidirectional communication range of the relay coil [10]. However, this strategy does not maximize the mutual induction, since $|M_{\text{horizontal}}| = 2 \cdot |M_{\text{vertical}}|$ according to (3). For $|Z| \gg |j2\pi fM|$ and $|x| \gg 1$, $F(x, k)$ can be approximated by $F(x, k) \approx x^k = \left(\frac{Z}{j2\pi fM} \right)^k$. Hence, we conclude from (20), that the pathloss is dramatically higher for vertical axes deployment, namely

$$L_{p,\text{vertical}}(f) \approx 2^{2k} \cdot L_{p,\text{horizontal}}(f). \quad (36)$$

Therefore, in the following, we assume horizontal axes deployment.

To gain some insight into optimization problem (34), we show

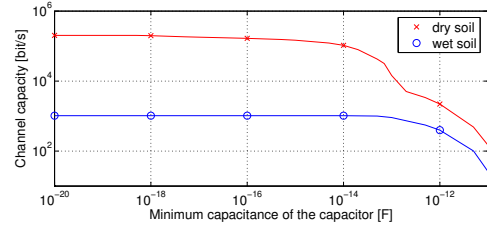


Fig. 5. Channel capacity vs. minimum capacitance of the capacitor.

in Fig. 4a) the channel capacity as a function of the carrier frequency for $N = 1000$. We assume an MI-waveguide with 15 relays and a total transmission distance of 50 m in dry soil. The channel capacities with and without the constrained capacitance $C_0 = 1$ pF (“With CC” and “Without CC” in Fig. 4, respectively) are shown. We observe that the maximum channel capacity is much lower if the capacitance is constrained. For the unconstrained solution, the channel capacity increases at high frequencies. This results from the fact that the skin depth in (4) converges to $\delta_{(f \rightarrow \infty)} = \frac{2}{\sigma \sqrt{\mu \epsilon}}$ and the soil becomes then a poor conductor. We also note that Fig. 4a) shows that the channel capacity is not convex in f_0 . In Fig. 4b), we show the channel capacity as a function of the number of windings for a constant carrier frequency $f_0 = 1$ MHz. Here, we again observe a performance degradation for the capacitor constrained optimization compared to the unconstrained optimization. From Fig. 4 we conclude that f_0 and N have to be jointly optimized. For the following results, this joint optimization was performed using the algorithm proposed in Section III-B.

In Fig. 5, the optimized channel capacity is depicted for an MI-waveguide with 15 relays and a total distance of 50 m as a function of the minimum capacitance C_0 . The number of iterations $X_I = 4$ appeared to provide sufficient precision of the optimization result. We observe that for dry soil, the decrease of the channel capacity for larger C_0 is more significant than for wet soil. Due to the low conductivity σ of dry soil, a high value of G close to one results and a higher frequency improves the coupling. This means that MI-waveguides for dry soil or small distances between coils have a low pathloss at high frequencies. MI-waveguides for wet soil or long distances between the coils have a low pathloss at lower frequencies, because the skin effect dominates the coupling properties. If we restrict the capacitance, the MI-waveguide has to operate at low frequency. This yields a dramatic degradation of performance in dry soil. This effect was neglected in [5] and [10]. In contrast, the influence of the capacitor constraint on the performance in wet soil is small (compared to the dry soil), because the maximal available carrier frequency due to the capacitor constraint is not significantly lower than the optimal carrier frequency for the unconstrained case. For very low minimum capacitances C_0 , the channel capacity converges to the unconstrained solution of (34).

For system design, we need to compare the performance of different MI-waveguide configurations. Therefore, we consider the channel capacities of the waveguides for different inter-relay distances. The minimum capacitance of the capacitor is set to $C_0 = 1$ pF. For comparison, we also show the channel capacity for EM-wave based communication with carrier fre-

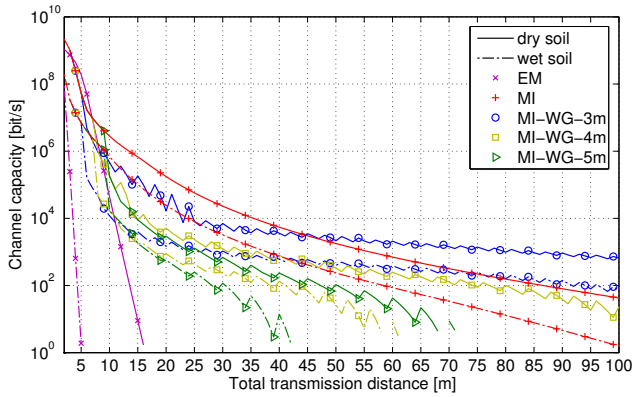


Fig. 6. Channel capacity of different MI-WUSNs and EM-wave transmission.

quency $f_0 = 300$ MHz and bandwidth $B = 100$ MHz, which is a suitable frequency band with low pathloss for EM-waves [4]. The noise power for EM based transmission is given by $P_{\text{noise,EM}} = KTB$ [16]. For the EM-waves, we assume free-space pathloss and the pathloss due to eddy currents as the only influences of the environment on the link. If additional effects like absorption and reflexion were included, the results for EM-wave transmission might become worse. For MI-WUSNs, we study four different constellations: MI without relaying (direct MI, or just “MI” in the figure), MI-waveguides with a minimum distance of 3 m, 4 m, and 5 m between coils (“MI-WG-3m”, “MI-WG-4m”, and “MI-WG-5m” in the figure). Minimum distance means that the highest possible number of relays, for which the intercoil distance is greater or equal to this minimum value, is selected. The results are depicted in Fig. 6. Remarkably, EM based transmission in dry soil is only beneficial for distances $d < 7$ m. In wet soil, the channel capacity of EM based transmission is always lower than that of MI-WUSNs. We note that due to the capacitor constraint the performance of the MI-waveguides is significantly reduced and may even fall below the channel capacity of the direct MI transmission. In fact, MI-waveguides with low relay densities (4 m or 5 m minimum intercoil distance) perform worse than direct MI transmission. This means that the deployment of the relay devices in MI-waveguides with low relay densities can even reduce the performance of the MI-WUSN. MI-waveguides with high relay densities (3 m minimum intercoil distance) are beneficial for distances $d > 45$ m. However, although MI-waveguides with 3 m intercoil distance can provide up to 600 bit/s for 100 m distance between the transceivers in dry soil, and therefore perform better than direct MI transmission, we need to consider the effort of deploying 32 relay coils and adjusting the angles between them, according to the horizontal axes deployment discussed earlier. The tradeoff between this effort and the relay efficiency is beyond the scope of this work and remains for future investigations.

V. CONCLUSION

In this paper, we derived novel channel and noise models for MI-based WUSNs. These models comprise not only the free-space attenuation of the MI-signals but also the loss due to eddy currents in the soil, which enables a more accurate system design. We presented two deployment strategies, horizontal and

vertical axes deployment, and have shown that the latter has a dramatically higher pathloss. We formulated an optimization problem for maximizing the channel capacity under practical design constraints and found a close-to-optimum solution via numerical evaluation in a given parameter space. It turns out that a constraint on the capacitance of the capacitor causes a significant degradation in performance of MI-waveguides. We compared the calculated channel capacities of direct MI transmission with that of MI-waveguides, and found that MI-waveguides with high relay densities are beneficial for inter-node distances larger than 45 m. In contrast, the channel capacity of MI-waveguides with low relay density is always lower than that of the direct MI transmission.

ACKNOWLEDGEMENTS

The authors would like to express their gratitude to Dr. H. Roßmanith for valuable discussions on the theory of electromagnetism.

REFERENCES

- [1] I.F. Akyildiz, W. Su, Y. Sankarasubramaniam, and E. Cayirci, “Wireless sensor networks: A survey,” *Comput. Netw. J.*, vol. 38, pp. 393–422, March 2002.
- [2] I.F. Akyildiz and E.P. Suntebeck, “Wireless underground sensor networks: Research challenges,” *Ad Hoc Netw. J.*, vol. 4, pp. 669–686, July 2006.
- [3] I.F. Akyildiz, Z. Sun, and M.C. Vuran, “Signal propagation techniques for wireless underground communication networks,” *Physical Communication Journal (Elsevier)*, vol. 2, pp. 167–183, September 2009.
- [4] L. Li, M.C. Vuran, and I.F. Akyildiz, “Characteristics of underground channel for wireless underground sensor networks,” in *Proc. IFIP Mediterranean Ad Hoc Networking Workshop (Med-Hoc-Net 07)*, Corfu, Greece, June 2007.
- [5] Z. Sun and I.F. Akyildiz, “Magnetic induction communications for wireless underground sensor networks,” *IEEE Trans. on Antennas and Propag.*, vol. 58, pp. 2426–2435, July 2010.
- [6] A. Karalis, J.D. Joannopoulos, and M. Soljacic, “Efficient wireless non-radiative mid-range energy transfer,” *Annals of Physics*, vol. 323, pp. 34–48, January 2008.
- [7] R.R.A. Syms, I.R. Young, and L. Solymar, “Low-loss magneto-inductive waveguides,” *Journal of Physics D: Applied Physics*, vol. 39, pp. 3945–3951, September 2006.
- [8] V.A. Kalinin, K.H. Ringhofer, and L. Solymar, “Magneto-inductive waves in one, two and three dimensions,” *Journal of Applied Physics*, vol. 92, no. 10, pp. 6252–6261, November 2002.
- [9] R.R.A. Syms and L. Solymar, “Noise in metamaterials,” *Journal of Applied Physics*, vol. 109, no. 124909, June 2011.
- [10] Z. Sun and I.F. Akyildiz, “On capacity of magnetic induction-based wireless underground sensor networks,” in *Proceedings of IEEE INFOCOM 2012*, March 2012, pp. 370–378.
- [11] H.-W. Beckmann, K. Lampe, H. Milde, H. Rohlfing, M. Scheurmann, F. Tornau, and F.-P. Zantis, *Friedrich Tabellenbuch Elektrotechnik/Elektronik*. Ferd. Dümmlers Verlag, 553.-579. Auflage, 1998.
- [12] H. Lindner, H. Brauer, and C. Lehmann, *Taschenbuch der Elektrotechnik und Elektronik*. Fachbuchverlag Leipzig, 8. Auflage, 2004.
- [13] E.E. Kriezis, T.D. Tsiboukis, S.M. Panas, and J.A. Tegopoulos, “Eddy currents: Theory and applications,” *Proceedings of the IEEE*, vol. 80, pp. 1559–1589, October 1992.
- [14] C. Jordan and K.G. Balmain, *Electromagnetic waves and radiating systems*, 2nd ed. Prentice-Hall, New Jersey, 1968.
- [15] S.J. Orfanidis, *Electromagnetic waves and antennas*. Piscataway, NJ: Rutgers Univ. Press, Last Revision August 2010.
- [16] H.T. Friis, “Noise figures of radio receivers,” *Proceedings of the IRE*, vol. 32, pp. 419–422, July 1944.
- [17] D. Tse and P. Viswanath, *Fundamentals of Wireless Communication*. Cambridge University Press, 2005.
- [18] S. Mei and Y.I. Ismail, “Modeling skin and proximity effects with reduced realizable RL circuits,” *IEEE Trans. on Very Large Scale Integration (VLSI) Systems*, vol. 12, no. 4, pp. 437–447, April 2004.
- [19] R.L. Spyker and R.M. Nelms, “Classical equivalent circuit parameters for a double-layer capacitor,” *IEEE Trans. on Aerospace and Electronic Systems*, vol. 36, pp. 829–836, July 2000.
- [20] S. Boyd and L. Vandenberghe, *Convex Optimization*. Cambridge University Press, 2004.